



# A novel approach to construct self-assembled 3D MEMS arrays

Sapida Akhundzada<sup>1,2,7</sup> · Xiaohui Yang<sup>1,3,7</sup> · Johannes Fiedler<sup>4,5</sup> · Eireen Käkel<sup>1,7</sup> · Basim Al-Qargholi<sup>1,6</sup> · Stefan Buhmann<sup>2,7</sup> · Arno Ehresmann<sup>2,7</sup> · Hartmut Hillmer<sup>1,7</sup>

Received: 1 February 2022 / Accepted: 3 August 2022 / Published online: 20 August 2022  
© The Author(s) 2022

## Abstract

The paper presents the design and technological fabrication process of Yin or Yang-shaped, micron-sized electromechanical system (MEMS) elements displaying asymmetric hollow cylinders with two different curvatures of the cylinder shell. By adapting the process steps, two neighboring shutter MEMS elements can either be attached to each other to create asymmetric hollow cylinders or remain disconnected to form curled cylindrical or ellipsoidal tubes or tube fractions. A novel 3D self-organization process has been developed to connect two neighboring shutter elements, exploiting surface tension forces via a sequential drying process. The process conditions have been analyzed and optimized to fabricate the two different geometries of the MEMS elements. The resulting MEMS system elements were characterized by focused ion beam and scanning electron microscopy. The contribution of Casimir force, van der Waals force, and other physical interfacial forces are discussed in the formation of the asymmetric hollow cylinders.

## 1 Introduction

Microelectromechanical systems (MEMS) for light processing have been studied for various applications. Among others, micromirror array-based MEMS have been reported for (1) NxN switches in wavelength division multiplexing (Chuan Pu et al. 2000; Lin and Goldstein 2002; Aksyuk et al. 2003), (2) for beamers (Duncan et al. 2002; Ballard

et al. 2016) and (3) for light steering via smart glazing in buildings (Hillmer et al. 2018, 2021; Iskhandar et al. 2019). In adaptive optics, deformable mirrors were developed, providing high-order correction of optical aberrations used in astronomy, laser micromachining, maskless lithography, microscopy medical technology, and optical free-space communication (Bifano 2011; Manzanera et al. 2011). These mirror elements are planar and electrostatically actuatable. As a side note, there are also some adaptive optics based on freeform reflectors (Doble and Williams 2004; Zhu et al. 2006).

Furthermore, shutter array-based MEMS have been reported for transmission-modulated smart glass (Lamontagne et al. 2009; Schlam et al. 2017), space instrumentation (Lamontagne et al. 2019), camera shutters (Kim and Hong 2011), and displays (Pizzi et al. 2003; Roux et al. 2005; Schalberger et al. 2016). Due to intrinsic stress, these shutter elements are curled in their default state and are uncurled by electrostatic actuation to obtain a flat configuration. In such shutter arrays, all elements possess the same curvature characteristics, acting in the same way upon external forces.

MEMS often suffer from stiction which, in most cases, is an undesired adhesion of structures having a large surface-to-volume ratio. Stiction can occur already after drying the MEMS structures or after snap-down (pull-in effect) initiated by electrostatic actuation. Then restoring forces embedded via stress are not able to overcome the

✉ Sapida Akhundzada  
s.akhundzada@physik.uni-kassel.de

<sup>1</sup> Institute of Nanostructure Technologies and Analytics (INA), University of Kassel, Heinrich-Plett-Str. 40, 34132 Kassel, Germany

<sup>2</sup> Institute of Physics, University of Kassel, Heinrich-Plett-Str. 40, 34132 Kassel, Germany

<sup>3</sup> Qingdao University of Science and Technology, Sino German Technical University, Songling Road, Qingdao, People's Republic of China

<sup>4</sup> Department of Physics and Technology, University of Bergen, Allegaten 55, 5007 Bergen, Norway

<sup>5</sup> Institute of Physics, University of Freiburg, Hermann-Herder-Str. 3, 79104 Freiburg, Germany

<sup>6</sup> Department of Biomedical Engineering, Al-Mustaqbal University College, Al-Najaf Street 10, 51001 Hillah, Iraq

<sup>7</sup> Centre for Interdisciplinary Nanostructure Science and Technology (CINSaT), University of Kassel, Heinrich-Plett-Str. 40, 34132 Kassel, Germany

interfacial forces such as capillary, electrostatic, Casimir, and van der Waals (Maboudian 2001). Many strategies have been reported to overcome the stiction effect in MEMS, such as anti-stiction layers (Ashurst et al. 2003; Petruzzella et al. 2018), geometry effects or further material effects.

The Casimir effect (Casimir 1948; Casimir and Polder 1948) was postulated in 1948 by Casimir and experimentally observed by Lamoreaux almost 50 years later (Lamoreaux 1997). It has attracted enormous attention from a fundamental point of view, where different scenarios, materials, and geometries have been investigated in the past (Capasso et al. 2007; Munday et al. 2009; Buhmann and Scheel 2009; Rodriguez et al. 2011; Reid et al. 2013; Tang et al. 2017; Zhao et al. 2019; Gong et al. 2020; Wang et al. 2021).

Conclusively, the construction of 3D structures is thematized. 3D microstructures with complex geometries have been implemented e.g. by micro-Origami and micro-Kirigami, which are inspired by the corresponding traditional Japanese folding and cutting techniques (Xu et al. 2017). By using different fabrication techniques like thin-film lithography, strain engineering and plastic relaxation via ion processing, complex self-organized 3D structures have been fabricated (Chalapat et al. 2013; Xi et al. 2014). These structures are tailored by 3D stress which is alone sufficient to hold them together without the need of being “glued” together.

Despite being a challenge for most MEMS applications, stiction is essential for our application to attach or “glue” MEMS blades together for forming complex 3D structures. Here we present a novel 3D self-organization methodology leading to the formation of heterogeneously curved hollow cylindrical elements, where two neighboring shutters have been connected to each other at their ends. The paper is organized as follows: Sect. 2 describes the two different geometries of the MEMS elements, where they are either individually curled or the neighboring elements are connected, forming 3D hollow elements with two parts of different curvature signs. Section 3 provides an overview of the fabrication technology, describing the different experimental conditions required for the two configurations in detail. Section 4 presents selected experimental results of both MEMS element configurations. In Sect. 5, the paper is concluded with a discussion about the physical effects contributing to the formation of the Yin or Yang-shaped elements.


## 2 Periodic arrangements of curled shutter elements and 3D asymmetric hollow cylinders

In this paper, we demonstrate the generation of 3D hollow MEMS elements having a cross-section similar to a Yin or Yang<sup>1</sup> shape, which shall be briefly named “asymmetric hollow cylinders” throughout this paper. They are formed by pairing two neighboring shutter elements. Depending on the technological fabrication process, we were able to generate either (1) a shutter element array of 20,000 shutters where all elements are curled in the same way or (2) an element array of 10,000 asymmetric hollow cylinders where each hollow cylinder is formed by two paired neighboring shutters. These elements possess the potential to be applied in sensors based on particle transport through confined channels (Ueltzhöffer et al. 2016), smart storage (Griffin et al. 2000), and transportation systems (Desai et al. 1999), where additional functionalization of the MEMS elements may be integrated.

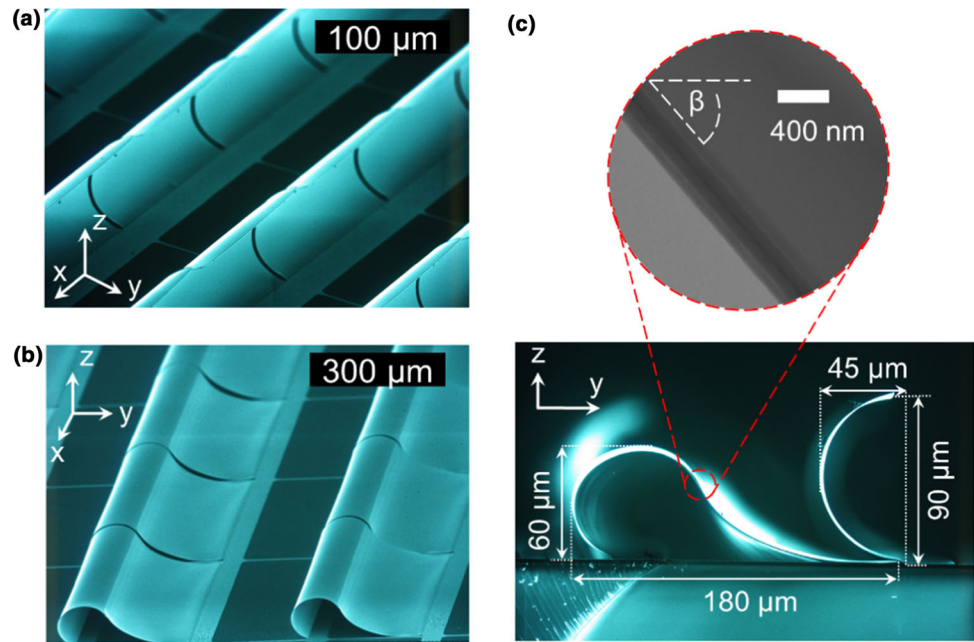
Figure 1a depicts an arrangement of curled open, free-standing shutter elements. Each element has been fixed to the substrate by an anchoring stripe and is curled with the same curvature, homogeneous within each element. The bending of the elements originates from different layer stresses in a bilayer or multilayer system, which is in the present case being implemented by an Al/Cr/Al layer system. In case of larger stress differences, each shutter can curl entirely and form a complete cylinder. This has been described several times in the literature (Tarraf et al. 2004; Mei et al. 2008; Takahashi et al. 2012).

Figure 1b shows an example of two neighboring elements being connected. They geometrically form an asymmetric hollow cylinder fabricated in a periodic arrangement. To the best of our knowledge, the corresponding method using the interaction between neighboring elements has not been suggested and carried out in a reproducible way before.

Figure 1c shows the cross-section of an asymmetric hollow cylinder in comparison to a curled unpaired micro shutter. That SEM image indicating the characteristic sizes of both types of MEMS structures (i.e., paired and unpaired elements on the same SEM micrograph) is obtained through cleaving and breaking the glass substrate. In that way, the shutters at the breaking edge—which were initially paired—are now separated by the cleavage and form unpaired (individual) elements, whereas the following

<sup>1</sup> Yin-Yang , from Chinese nature philosophy, symbolizing a concept of dualism. The two black and white objects describe how seemingly opposite or contrary forces may actually be complementary, interconnected, and interdependent in the natural world. (“The unlike is joined together, and from differences results the most beautiful harmony.”; Heraclitus; c. 535—c. 475 BC).

**Fig. 1** Scanning electron microscopy (SEM) images of the fabricated MEMS elements: **a** Identical and homogeneously curled elements, **b** periodic arrangement of asymmetric hollow cylinders fabricated by connecting two neighboring elements to form one MEMS element. **c** Cross-sections of both types of MEMS structures are marked with corresponding geometrical sizes. The inset shows the overlapping region of the two shutters. In all our experiments, we have identified an identical tilt angle  $\beta = 53^\circ$



paired micro shutter elements in the same row remain in their connected state.

### 3 Materials and methods

#### 3.1 Fabrication technology

For the fabrication of the shutter elements, first, (1) an optical lithography process is conducted to define the rectangular geometry of the shutter MEMS elements with lateral dimensions of  $150 \times 400 \mu\text{m}$ . In the next step (2), thin films of aluminum (Al) and chromium (Cr) are deposited by electron beam physical vapor deposition. The layer system consisting of 99 nm Al, 16 nm Cr and 88 nm Al is deposited with deposition rates of 0.3 nm/s. This layer stack is utilized for initiating intrinsic stress leading to free-standing shutter elements after (3) dissolving the resist sacrificial layer by *N*-Methyl-2-pyrrolidone during the lift-off process. For removal of resist residuals, the sample is immersed in an isopropanol bath and subsequently (4) the MEMS elements are dried using a specific drying technique established in our labs. The details of this very last drying step define whether free-standing unpaired micro shutters or paired elements are obtained. These will be described in the following sections. A schematic sketch of the fabrication procedure is added to the supplementary material. Note that the abovementioned numerals (1–4) are used to depict the processing sequence.

#### 3.2 Standard drying process for identical curled and homogeneously curved elements

For the standard drying process, a circular glass tank with a radius of 10 cm and a height of 15 cm is filled with isopropanol and placed on a hotplate set to  $80^\circ\text{C}$ . The sample containing the shutter elements is placed inside the glass tank. At the sample position, the isopropanol has a temperature of  $65.0 \pm 0.5^\circ\text{C}$ . The glass tank (Fig. 2a) is equipped with a steam bell on top. The evaporating isopropanol is kept inside by closing the steam bell valve. The atmosphere above the isopropanol bath inside the steam bell became enriched with gaseous isopropanol, resulting in a steady increase in partial and absolute pressures. The increasing pressure pushes liquid isopropanol through the lower circular end of the steam bell in radial directions sides as shown in Fig. 2b. The main idea of this drying process is to realize a defined transfer of the sample from liquid isopropanol to an atmosphere containing gaseous isopropanol, which is important for stabilizing the shapes of the paired or unpaired shutter elements. The curled elements are pulled down by the surface tension of the thinning liquid isopropanol film (Fig. 2c). Once the liquid has evaporated completely, the micro shutter elements do not remain in this state as the intrinsic stress is large enough to cause the curling of the shutter elements again. This process occurs in a period of a few seconds (Fig. 2d). The dried shutter elements, having a homogenous and identical shape in the array, are surrounded by gaseous isopropanol. A possible temperature gradient in the gaseous isopropanol does not influence the shape of the shutter elements, therefore, is not relevant for the drying process.

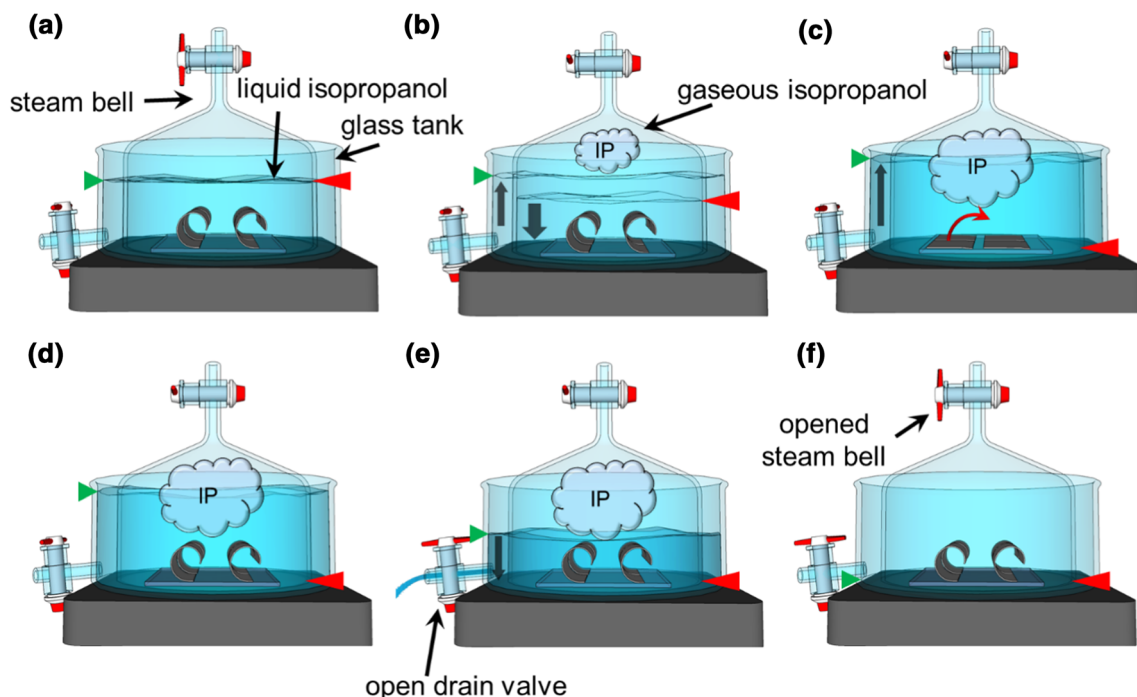


**Fig. 2** Drying process for identical homogeneously curved elements with horizontal substrates. After warming up the setup, **a** the valve of the steam bell is closed and the evaporating isopropanol (IP) is trapped inside, resulting in **b** an increased pressure inside the glass container. Thereby, the isopropanol is pushed outside, leading to the drying of the micro shutters. **c** A narrowing liquid isopropanol film pulls down the curled shutter elements to a flat shape, but **d** the micro

shutters are rolled up again due to the intrinsic stress in their metal layers once the liquid has evaporated completely. **e** The valve of the glass tank is then opened to remove the pushed-out isopropanol and **f** the valve of the steam bell is opened to exchange the atmosphere inside the glass steam bell. The isopropanol fill levels inside and outside the steam bell are labeled by red and green arrows respectively

After the liquid isopropanol is pushed completely outside the steam bell, it is subsequently removed by opening the drain valve of the glass tank (Fig. 2e). Finally, the valve of the steam bell is opened for exchanging the isopropanol atmosphere with air and the sample is taken out of the glass tank (Fig. 2f). The results are free-standing and unpaired curled shutter elements. As can be observed in SEM shown in Fig. 1a, all shutter elements exhibit homogeneous curvature in the open state.

### 3.3 Modified drying process to fabricate paired elements

As depicted in Fig. 1b, we used a distinct modification of the drying process to achieve paired shutter elements forming asymmetric hollow cylinders. We tilted the sample inside the glass container, resulting in a wedged liquid isopropanol depth and a gradual drying process. This is implemented by utilizing a wedge-shaped aluminum block with an angle of  $10^\circ$  underneath the sample, as shown in Figs. 3a, 4a. A photo of our setup is shown in Fig. 4b. In comparison to the standard procedure, the hotplate was set to  $90^\circ\text{C}$ , resulting in a liquid temperature of  $68.5 \pm 0.5^\circ\text{C}$ . As schematically shown in Fig. 3a, the

shutter elements of row I will dry first, while elements of row II will still be covered by a liquid isopropanol film. The elements of row I are therefore pulled down by the surface tension of the thinning liquid film until they get in contact with the elements of row II, which had not changed their curvature characteristics (Fig. 3b). The interaction forces between the two MEMS elements have been observed to be stronger than the surface tension forces exerted on elements of row II by the thinning liquid film and stronger than the intrinsic stress (of the elements of row I) which is trying to roll up the elements of row I (Fig. 3c). Therefore, the two neighboring elements stay joined after the drying process (Fig. 3d, e). Possible forces involved in maintaining the sticking of neighboring shutters will be discussed in the upcoming Sect. 5. The sticking between these two neighboring shutter elements leads to the formation of asymmetric hollow cylinders (Fig. 1c). This self-formation process continues for consecutive rows of elements, leading to a periodic formation of hollow cylinders. Macroscopically, this process can be observed when the liquid–gas interface moves downwards with an initial speed of  $0.3\text{ mm/s}$  and ends at a speed of  $0.1\text{ mm/s}$  since the ratio of liquid isopropanol to gaseous isopropanol

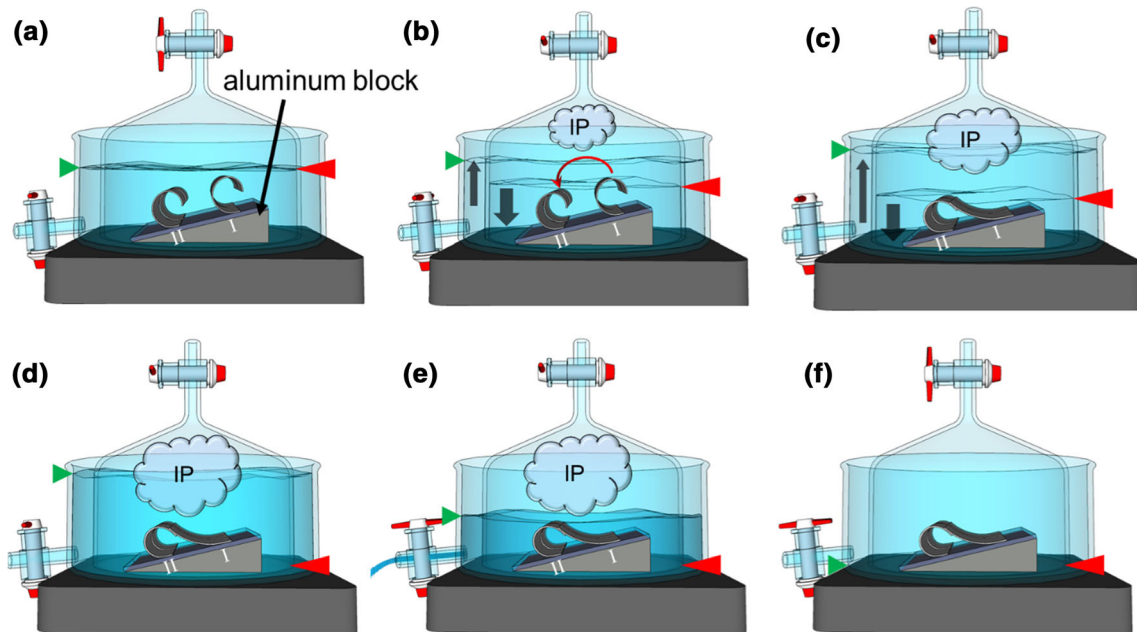


**Fig. 3** Sketch of the fabrication of asymmetric hollow cylinders consisting of paired micro shutters involving tilted substrates. Due to the **a** tilted position, **b** the isopropanol is drying gradually on the substrate’s surface. As the elements of row I are dried, **c** they are pulled down and come in contact with the micro shutters from row II that are still in their curled form as they are still immersed in the liquid isopropanol. The gradual drying process results in the periodic

formation of asymmetric hollow cylinders. **d** At the end of the drying process where liquid isopropanol is pushed out of the steam bell, **e** the valve of the glass tank is opened to remove the isopropanol. **f** Finally, the valve of the steam bell is opened to exchange the atmosphere inside the glass steam bell. The isopropanol fill levels inside and outside the steam bell are labeled by red and green arrows respectively

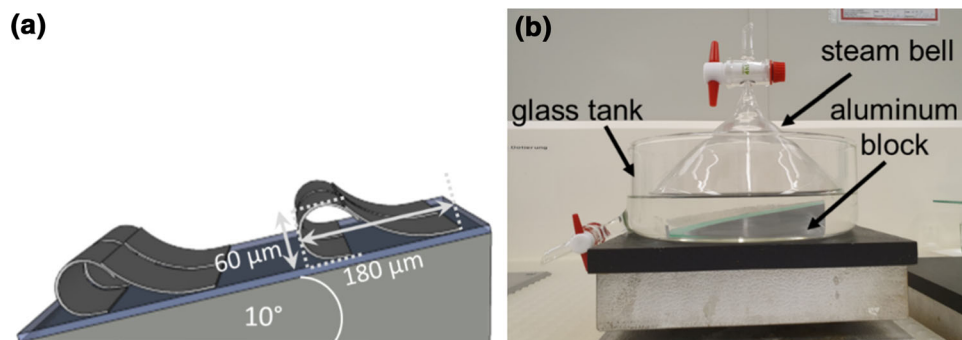


**Fig. 4 a** Sketch of asymmetric hollow cylinders placed on top of an aluminum wedge used during the drying process, including their corresponding geometrical sizes. **b** A photo of the drying setup which

is used for the fabrication of asymmetric hollow cylinders consisting of a circular glass tank, steam bell, and aluminum wedge

inside the glass steam bell has changed in comparison to the starting point.

### 4 Experimental results

For unpaired curled elements, it is crucial to position the sample without any tilt inside the glass container before starting the drying process. Our experiments showed that a thin isopropanol film remaining on the sample surface causes a change in the micro shutters’ shape if it is not spread homogeneously. Figure 1c depicts the shape of the

unpaired micro shutters having a radius of approximately 45 μm. The shutter’s curvature is slightly changing over time due to an oxidation process of the metallic layers in an oxygen-containing atmosphere.

In the case of paired elements forming asymmetric hollow cylinders, our experiments indicated that the pairing only occurs if the orientation of the sample is set like in Fig. 3a. Rotating the sample by an angle of 90° in plane leads to an inhomogeneous and non-periodic formation of the asymmetric cylinders, while a rotation of 180° effectively prevents the hollow cylinder formation. After the drying process, the shape of the asymmetric hollow

cylinders is stable and does not change over time. The asymmetric hollow cylinders, consisting of two micro shutter elements as depicted in Fig. 1c, possess on average a width of 180  $\mu\text{m}$  and a height of 60  $\mu\text{m}$ . As the design of the elements and the arrangement of the cylinders are periodic, the length of the hollow cylinders depends only on the size of the MEMS shutter and the substrate size.

For electrostatic actuation experiments, the micro shutters and the asymmetric hollow cylinders are fabricated on top of glass substrates covered with a 650 nm thick layer of fluorine-doped tin oxide (FTO) used as a transparent electrode and a 1  $\mu\text{m}$  thin insulating layer of silicon dioxide. An external voltage is applied between the MEMS structures and the conductive layer underneath. With increasing voltage, the curvature of micro shutters is gradually reduced due to the electrostatic force pulling them down towards the conductive FTO layer under the substrate surface. Above a threshold voltage of approximately 40 V, the micro shutters are resting flat on the substrate surface. The shutters will curl back to their initial configuration when the applied voltage is reduced to a certain threshold. This behavior is already well known from our micromirror elements (Hillmer et al. 2018, 2021; Iskhandar et al. 2019). In the case of the asymmetric hollow cylinders reported here, the paired micro shutters could not be separated again—even with massive electrostatic actuation (100 V).

## 5 Discussion

The formation of the asymmetric hollow cylinders is a special phenomenon being influenced by different forces during the pairing process of two neighboring elements. The initial driving force is related to the surface tension of the isopropanol as it is wetting the entire sample surface at the beginning of the modified drying process. Due to the tilted position of the micro shutters, the surface tension pulls down the shutters until they are within immediate vicinity of their neighbors in the next row. Using focused ion beam (FIB), we etched several trenches in the region where the two shutter blades overlap (Figs. 1c and 5e). Subsequent scanning electron microscopy (SEM) measurements show the cross sections of the Al-Cr-Al-gap-Al-Cr-Al stacks and reveal an average distance (gap) of about  $d \approx 10$  nm between the two shutter blades attached to each other (see supplementary material). To maintain the pairing of two elements after removing the liquid completely, Casimir forces, Van der Waals forces and electrostatic forces may be involved.

During the drying process, the moving electrical dipoles in isopropanol could charge the metallic blades. However, this effect might be negligible in our case, since our

experimental findings (Fig. 1b, shutter pairing) are not supporting it (see supplementary material). The dipole–dipole interaction, known as Van der Waals attraction, might already reveal stronger forces in our case. Not all isopropanol might be removed during the drying process, especially not those remaining between the two metallic blades.

Notwithstanding, in our experiments, we believe that Casimir forces are dominating in attaching neighboring shutter blades together—remarkably stable over time. Casimir forces can be attractive or repulsive, depending on the distance between the plates and the relative magnitudes of the permittivity values of the three materials involved (Munday and Capasso 2007; Reid et al. 2013; Zhao et al. 2019). In most cases, they are attractive and bring two metallic plates closer to each other, compensating e.g. elastic counterforces (restoring forces). In the case of Casimir's original setup consisting of two perfectly conducting plates in vacuum (Casimir 1948; Casimir and Polder 1948), this attraction can intuitively be understood in terms of virtual photon pressure: Since we have less quantum fluctuations between the two plates (cavity) than the outside, forces on both Al blades (resulting from photon momentum transfers to the plates) are directed towards the center. This means that we have a smaller photon density of states inside the cavity than the outside. The vacuum fluctuations can be interpreted as spontaneously generated and vanishing virtual particles. Finally, this is a consequence of Einstein's  $E = mc^2$ , Heisenberg's uncertainty relation, the wave-particle duality, and the fact that particles have a non-vanishing zero-point energy. Following Casimir's seminal work, many studies have revealed the existence of Casimir forces outside vacuum, e.g. in fluids (Munday and Capasso 2007; Zhao et al. 2019). Any dielectric fluid medium (liquid, gas) between the plates will enable modes and exhibits the Casimir effect. Various material combination of objects and fluids have been investigated in the meantime.

Due to our specific drying process (angled configuration, Fig. 3), surface tension forces bring the two neighboring blades close together. At the end of the drying process where the liquid between the blades disappears almost completely, the blades are approaching more closer to each other. After drying, Casimir forces most probably keep the blades connected in a stable configuration, stabilizing the asymmetric hollow cylinders. If residues of isopropanol molecules remain between the metallic blades, Van der Waals forces could also contribute to the attraction of the two blades. Note that Casimir forces can also be theoretically deducted from relativistic van der Waals forces between fluctuating dipoles, as an alternative to the derivation by Casimir (Lifshitz 1992). Casimir forces

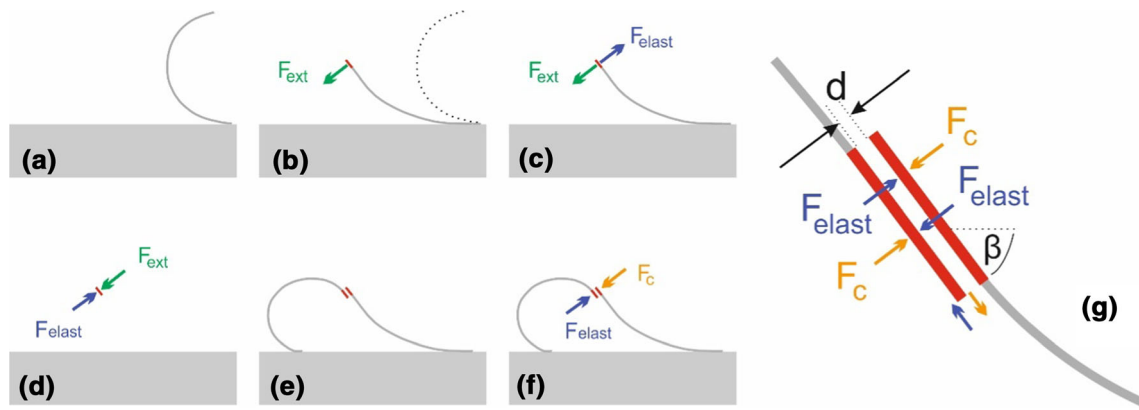


**Fig. 5** Simulation steps to estimate the distance  $d$ . **a** Unactuated shutter, **b** unactuated shutter (dotted) and shutter (full line) actuated via an external force  $F_{ext}$  acting on the area  $A$  (its cross section highlighted as a red stripe), **c** elastic force  $F_{elast}$  and counteracting external force  $F_{ext}$  on area  $A$ , **d** the identical force equilibrium with the same but shifted forces, **e** both shutters in grey overlapping within

**A** (red), **f** force equilibrium for the right shutter: restoring elastic force  $F_{elast}$  and counteracting Casimir force  $F_C$ , acting on the right area  $A$ (red), **g** force equilibrium involving also forces acting on the left shutter and formation of a plate capacitor arrangement (red) with known area  $A$  and distance  $d$  to be determined

strongly grow with decreasing distance  $d$ . We believe that the existence of the gas/liquid interface in combination with the tilted substrate orientation is crucial in our case to attach the neighboring shutters together. Additionally, theoretical model calculations are performed to identify whether the Casimir forces alone can compensate the restoring elastic forces for that specific force equilibrium observed in Fig. 1c. These simulations will be used to estimate the hypothetic distance  $d$  between the shutter blades necessary for blade sticking solely due to Casimir forces. The steps of the simulations are displayed in Fig. 5.

COMSOL™ Multiphysics (Multiphysics 1998) has been used to calculate the restoring forces. In Fig. 5a, an unpaired shutter is shown (unactuated state), corresponding to the right single shutter in the SEM micrograph of Fig. 1c. Now, an external force is used to actuate this shutter (Fig. 5b). The calculated restoring force continuously increases from the situation of an unactuated position (dotted in Fig. 5b) to the final specific position (full line in Fig. 5b), which represents and quantitatively corresponds to the bending of the paired situation displayed at the left side of Fig. 1c. This final position is again shown in Fig. 5c, displaying the force equilibrium between the external force  $F_{ext}$  and the restoring elastic force  $F_{elast}$ . SEM micrographs reveal an overlapping area of the neighboring shutter elements  $A = 4 \mu\text{m} \times 400 \mu\text{m} = 5600 \mu\text{m}^2$ , where the  $14 \mu\text{m}$  overlap is shown in red in Fig. 5. In our simulation on the basis of the involved materials, E-moduli, shutter geometry and thicknesses, an external force  $F_{ext} = 9 \cdot 10^{-6} \text{ N}$  would be required to bend the shutter into the specific position shown in Fig. 1c. In Fig. 5e, the two shutters overlap on area  $A$  (cross section shown as two red stripes) and illustrates the model used to estimate the hypothetic distance  $d$

between the shutter blades necessary for blade sticking solely by Casimir forces. As already mentioned, within the area  $A = 5600 \mu\text{m}^2$ ,  $F_{ext}$  is compensating the elastic force  $F_{elast}$  to reproduce the bending (Fig. 5c) observed in the SEM of Fig. 1c. Vectors can be shifted along their direction, which is done in Fig. 5d. The “plate capacitor” (red) with the known area  $A$  and the distance  $d$  of the gap to be determined are shown in Fig. 5e, together with the two shutter blades. Such procedure conveys the elastic force  $F_{elast}$  (blue) acting on the right area  $A$  (red) and allows for the right shutter to estimate the hypothetic balancing Casimir force  $F_C$  (orange), as shown in Fig. 5f. Figure 5g shows a sketch of the force equilibrium, including also the forces on the left shutter. In all our experiments, we identified an identical tilt angle  $\beta = 53^\circ$  of the plane (area  $A$ ), in which the two shutters overlap.

Three different approaches to calculate the Casimir force are used and compared in the following.

- Eq. (1) gives the formula derived by Casimir (1948) for ideally conducting and thus ideally reflecting (100%) parallel flat plates with no medium between the plates,

$$F_C = - \frac{\pi h c A}{480 d^4} \tag{1}$$

with the area of plate capacitor  $A$ , Planck’s constant  $h$ , distance  $d$  between the plates and vacuum light velocity  $c$ . A Casimir force of  $F_C = 9 \cdot 10^{-6} \text{ N}$  requires a gap distance  $d \leq 30 \text{ nm}$  to balance the elastic force  $F_{elast}$  for  $A = 5600 \mu\text{m}^2$ . Thus, our estimating simulation reveals that a tight attachment between the two shutters by Casimir forces would be possible if  $d \leq 30 \text{ nm}$ . This is consistent with our SEM

micrographs indicating a distance of about 10 nm or less. For this case, the simulated force density  $f$  is plotted as a function of  $d$  in Fig. 6 (red line).

- Next, the Casimir force is calculated in the non-retarded limit (van der Waals limit) in which the distance between the two plates is much smaller than  $c/\omega$ , where  $\omega$  is the angular frequency of the fluctuating dipoles. The Casimir force (1) considers perfectly reflecting plates, which is not appropriate for realistic materials that become transparent for high-energy radiation. To include this effect, we express the Casimir force via (Burger et al. 2020) as

$$F_c = -\frac{H A}{6\pi d^3} \quad (2)$$

where the Hamaker constant  $H$  depends on the dielectric function of the aluminium plates. The optical data have been taken from Adachi (2012), leading to a Hamaker constant of  $H = 4.554 \cdot 10^{-19}$  J, which is in agreement with the literature (Tolias 2020) within the common error bars. A Casimir force of  $F_c = 9 \cdot 10^{-6}$  N requires a gap distance  $d \leq 21.8$  nm to balance the elastic force  $F_{\text{elast}}$  for  $A = 5600 \mu\text{m}^2$ . Thus, a tight attachment between the two shutters by Casimir forces would be possible if  $d \leq 21.8$  nm. This is also consistent with our SEM micrographs. A fortiori, the measured gap distance  $d$  of about 10 nm between the two shutter blades would provide a much larger Casimir force. Thus, we believe that the two shutter blades are not only kept in balance but might also be pressed to each other more than 10-times stronger than required ( $22 \text{ nm}/10 \text{ nm} = 2.2$ , where  $2.2^3 = 10.6$ ). For this case, the simulated force density  $f$  is plotted as a function of  $d$  in Fig. 6 (blue dashed line).

- The third approach comprises the calculation of the exact Casimir force (Fiedler et al. 2020). For this case,

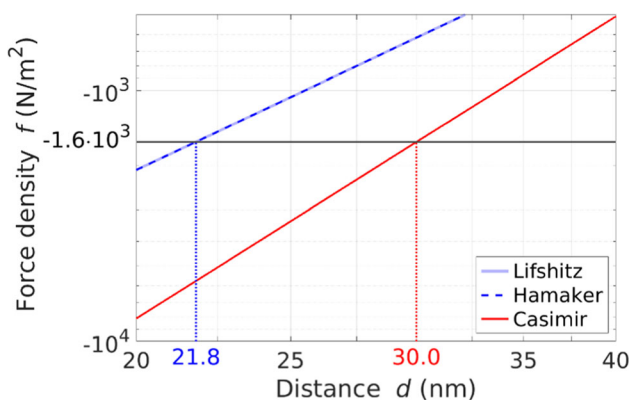


**Fig. 6** Model calculations of the obtained Casimir force densities depending on the distance between the shutter blades  $d$  for (1) the Casimir approach (red line), (2) the Hamaker approach (dashed blue line) and (3) the exact model (solid light blue line), respectively

the simulated force density is plotted in as a function of  $d$  in Fig. 6 (light blue full line). It can be observed that the Hamaker approximation almost exactly coincides with the Casimir force density in the relevant spatial region.

Note that this a rough estimate since we simulated with bulk E-Moduli, considered ideally flat parallel plates and neglected possible thin metal oxide layers on the surfaces. Details of the role of surface roughness, lateral forces, the role of the existence of a fluid/gas interface and the role of electrostatic forces is given in the supplementary material as well as details on geometrical and material data used in the simulation.

## 6 Conclusion

We presented a novel methodology to attach MEMS blades together. The applied liquid surface tension brings the two neighboring blades close to each other, which subsequently get attached to each other by the Casimir force. This could provide a novel fabrication method to build complex MEMS structures by attaching small parts of overlapping blades through a self-assembly methodology. We compare the results of two different MEMS fabrication options, obtaining different structural configurations of the MEMS elements: curled micro shutters and asymmetric hollow cylinders (paired shutters). The paired shutters reveal a Yin-Yang shape, exhibiting a constant overlap area between the two shutter blades, a constant opening and a constant radius at constant material thicknesses. The two configurations were generated via two different drying strategies as the last step of the fabrication procedure. Optimum operation settings for the reproducible fabrication of both MEMS elements have been developed. In future experiments, the influence of the process temperature on the yield and shape of the asymmetric hollow cylinders will be studied systematically. The attaching force keeping two neighboring micro shutters tightly fixed to a single non-circular cylinder is most probably of quantum photonic nature, namely the Casimir force. If the shutter blade distance is less or equal to 22 nm, the Casimir force would be strong enough for a strong adhesion, which is in agreement to SEM micrographs revealing an average gap distance of about 10 nm. Using the Casimir forces, we can build complex MEMS structures with interesting potential applications in microfluidic diagnostics, lab-on-chip technology and medical drug delivery.

**Supplementary Information** The online version contains supplementary material available at <https://doi.org/10.1007/s00542-022-05361-1>.



**Acknowledgements** The authors would like to thank G. Xu, C. Woitd, H. Wilke, H. Luo, M. Khan, J. Krumpolz, A. Friedrichsen, N. Körte, S. Baby, A. Nandakumar, T. Thomas, M. Smolarczyk, P. Kästner and R. Donatiello for fruitful discussions and technological support; as well as DBU (Nos. AZ23717, AZ20012/189, and AZ35501), and BMBF (Nos. 13N14517 and 13N15740) for financial support. The author S. A. acknowledges gratefully the support by the Ph.D. scholarship fund of Kassel university.

**Funding** Open Access funding enabled and organized by Projekt DEAL.

**Open Access** This article is licensed under a Creative Commons Attribution 4.0 International License, which permits use, sharing, adaptation, distribution and reproduction in any medium or format, as long as you give appropriate credit to the original author(s) and the source, provide a link to the Creative Commons licence, and indicate if changes were made. The images or other third party material in this article are included in the article's Creative Commons licence, unless indicated otherwise in a credit line to the material. If material is not included in the article's Creative Commons licence and your intended use is not permitted by statutory regulation or exceeds the permitted use, you will need to obtain permission directly from the copyright holder. To view a copy of this licence, visit <http://creativecommons.org/licenses/by/4.0/>.

## References

- Adachi S (2012) The handbook on optical constants of metals. World Scientific, Singapore
- Aksyuk VA, Pardo F, Carr D, Greywall D, Chan HB, Simon ME, Gasparyan A, Shea H, Lifton V, Bolle C, Arney S, Frahm R, Paczkowski M, Haueis M, Ryf R, Neilson DT, Kim J, Giles CR, Bishop D (2003) Beam-steering micromirrors for large optical cross-connects. *J Light Technol* 21:634–642. <https://doi.org/10.1109/JLT.2003.811792>
- Al-Qargholi B (2016) Development, evaluation and optimization of fabrication processes for daylight guiding systems based on micromirror Arrays. University of Kassel, Kassel
- Ashurst WR, Carraro C, Maboudian R (2003) Vapor phase anti-stiction coatings for MEMS. *IEEE Trans Dev Mater Reliab* 3:173–178. <https://doi.org/10.1109/TDMR.2003.821540>
- Ballard B, Bhakta V, Douglass M, Gelabert P, Kempf J, McDonald W, Pettitt G, Rancuret P, Rankin A, Thompson J, Oden PI (2016) ‘Steering’ light with texas instruments digital micromirror device (DMD)—past, present & future. *SID Symp Dig Tech Pap* 47:28–31. <https://doi.org/10.1002/sdtp.10590>
- Bifano T (2011) MEMS deformable mirrors. *Nat Photonics* 5:21–23. <https://doi.org/10.1038/nphoton.2010.297>
- Buhmann SY, Scheel S (2009) Nonequilibrium thermal Casimir–Polder forces. *Phys Scr T135:014013*. <https://doi.org/10.1088/0031-8949/2009/T135/014013>
- Burger FA, Corkery RW, Buhmann SY, Fiedler J (2020) Comparison of theory and experiments on van der waals forces in media—a survey. *J Phys Chem C* 124:24179–24186. <https://doi.org/10.1021/acs.jpcc.0c06748>
- Capasso F, Munday JN, Iannuzzi D, Chan HB (2007) Casimir forces and quantum electrodynamic torques: physics and nanomechanics. *IEEE J Sel Top Quant Electron* 13:400–414. <https://doi.org/10.1109/JSTQE.2007.893082>
- Casimir HBG (1948) On the attraction between two perfectly conducting plates. *Proc K Ned Akad* 51:793–796
- Casimir HBG, Polder D (1948) The influence of retardation on the London-van der waals forces. *Phys Rev* 73:360–372. <https://doi.org/10.1103/PhysRev.73.360>
- Chalapat K, Chekurov N, Jiang H, Li J, Parviz B, Paroanu GS (2013) Self-organized origami structures via ion-induced plastic strain. *Adv Mater* 25:91–95. <https://doi.org/10.1002/adma.201202549>
- Chuan Pu, Lin LY, Goldstein EL, Tkach RW (2000) Client-configurable eight-channel optical add/drop multiplexer using micromachining technology. *IEEE Photonics Technol Lett* 12:1665–1667. <https://doi.org/10.1109/68.896342>
- Desai A, Lee S-W, Tai Y-C (1999) A MEMS electrostatic particle transportation system. *Sensors Actuators A Phys* 73:37–44. [https://doi.org/10.1016/S0924-4247\(98\)00252-0](https://doi.org/10.1016/S0924-4247(98)00252-0)
- Doble N, Williams DR (2004) The application of MEMS technology for adaptive optics in vision science. *IEEE J Sel Top Quant Electron* 10:629–635. <https://doi.org/10.1109/JSTQE.2004.829202>
- Duncan WM, Bartlett T, Lee B, Powell D, Rancuret P, Sawyers B (2002) Dynamic optical filtering in DWDM systems using the DMD. *Solid State Electron* 46:1583–1585. [https://doi.org/10.1016/S0038-1101\(02\)00109-0](https://doi.org/10.1016/S0038-1101(02)00109-0)
- Fiedler J, Berland K, Spallek F, Brevik I, Persson C, Buhmann SY, Boström M (2020) Nontrivial retardation effects in dispersion forces: from anomalous distance dependence to novel traps. *Phys Rev B* 101:235424. <https://doi.org/10.1103/PhysRevB.101.235424>
- Gong T, Corrado MR, Mahbub AR, Sheldon C, Munday JN (2020) Recent progress in engineering the Casimir effect—applications to nanophotonics, nanomechanics, and chemistry. *Nanophotonics* 10:523–536. <https://doi.org/10.1515/nanoph-2020-0425>
- Griffin JL, Schlosser SW, Ganger GR, Nagle DF (2000) Modeling and performance of MEMS-based storage devices. *ACM SIGMETRICS Perform Eval Rev* 28:56–65. <https://doi.org/10.1145/345063.339354>
- Hillmer H, Al-Qargholi B, Khan MM, Worapattrakul N, Wilke H, Woitd C, Tatzel A (2018) Optical MEMS-based micromirror arrays for active light steering in smart windows. *Jpn J Appl Phys* 57:08PA07. <https://doi.org/10.7567/JJAP.57.08PA07>
- Hillmer HH, Iskandar MSQ, Hasan MK, Akhundzada S, Al-Qargholi B, Tatzel A (2021) MOEMS micromirror arrays in smart windows for daylight steering. *J Opt Microsyst*. <https://doi.org/10.1117/1.JOM.1.1.014502>
- Iskandar M, Al-Qargholi B, Khan M, Tatzel A, Luo H, Nazemroaya S, Li Q, Hillmer H (2019) Development of optical MEMS-based micromirror arrays for smart window applications: implementation of subfield addressing and reliability measurements. *Jahrb Oberfl* 75:93–107
- Kim C-H, Hong S (2011) Study on the reliability of the mechanical shutter utilizing roll actuators. In: 2011 IEEE 24th International conference on micro electro mechanical systems. IEEE, pp 501–504
- Kipp T, Welsch H, Strelow C, Heyn C, Heitmann D (2006) Optical modes in semiconductor microtube ring resonators. *Phys Rev Lett* 96:1–4. <https://doi.org/10.1103/PhysRevLett.96.077403>
- Klatt J, Barcellona P, Bennett R, Bokareva OS, Feth H, Rasch A, Reith P, Buhmann SY (2017) Strong van der waals adhesion of a polymer film on rough substrates. *Langmuir* 33:5298–5303. <https://doi.org/10.1021/acs.langmuir.7b01381>
- Lamontagne B, Barrios P, Py C, Nikumb S (2009) The next generation of switchable glass: the micro-blinds. *Proc Glas Perform Days* 2:637–639
- Lamontagne B, Fong NR, Song I-H, Ma P, Barrios P, Poitras D (2019) Review of microshutters for switchable glass. *J Micro/Nanolithog MEMS MOEMS* 18:1. <https://doi.org/10.1117/1.jmm.18.4.040901>

- Lamoreaux SK (1997) Demonstration of the Casimir force in the 0.6 to 6 $\mu$ m range. *Phys Rev Lett* 78:5–8. <https://doi.org/10.1103/PhysRevLett.78.5>
- Lifshitz EM (1992) The theory of molecular attractive forces between solids. *Perspectives in theoretical physics*. Elsevier, Amsterdam, pp 329–349
- Lin LY, Goldstein EL (2002) Opportunities and challenges for MEMS in lightwave communications. *IEEE J Sel Top Quantum Electron* 8:163–172. <https://doi.org/10.1109/2944.991412>
- Maboudian R (2001) Micro devices: stiction and adhesion. *Encyclopedia of materials: science and technology*. Elsevier, Amsterdam, pp 5591–5593
- Manzanera S, Helmbrecht MA, Kempf CJ, Roorda A (2011) MEMS segmented-based adaptive optics scanning laser ophthalmoscope. *Biomed Opt Express* 2:1204. <https://doi.org/10.1364/BOE.2.001204>
- Mei Y, Huang G, Solovev AA, Ureña EB, Mönch I, Ding F, Reindl T, Fu RKY, Chu PK, Schmidt OG (2008) Versatile approach for integrative and functionalized tubes by strain engineering of nanomembranes on polymers. *Adv Mater* 20:4085–4090. <https://doi.org/10.1002/adma.200801589>
- Mendach S, Kiravittaya S, Rastelli A, Benyoucef M, Songmuang R, Schmidt OG (2008) Bidirectional wavelength tuning of individual semiconductor quantum dots in a flexible rolled-up microtube. *Phys Rev B-Condens Matter Mater Phys* 78:2–5. <https://doi.org/10.1103/PhysRevB.78.035317>
- Multiphysics C (1998) Introduction to COMSOL multiphysics extregistered. COMSOL Multiphysics, Burlington, MA. Accessed 09 Feb 2018
- Munday JN, Capasso F (2007) Precision measurement of the Casimir–Lifshitz force in a fluid. *Phys Rev A* 75:060102. <https://doi.org/10.1103/PhysRevA.75.060102>
- Munday JN, Capasso F, Parsegian VA (2009) Measured long-range repulsive Casimir–Lifshitz forces. *Nature* 457:170–173. <https://doi.org/10.1038/nature07610>
- Petruzzella M, Zobenica Ž, Cotrufo M, Zardetto V, Mameli A, Pagliano F, Koelling S, van Otten FWM, Roozeboom F, Kessels WMM, van der Heijden RW, Fiore A (2018) Anti-stiction coating for mechanically tunable photonic crystal devices. *Opt Express* 26:3882. <https://doi.org/10.1364/OE.26.003882>
- Pizzi M, Koniachkine V, Nieri M, Sinesi S, Perlo P (2003) Electrostatically driven film light modulators for display applications. *Microsyst Technol* 10:17–21. <https://doi.org/10.1007/s00542-002-0244-0>
- Reid MTH, White J, Johnson SG (2013) Fluctuating surface currents: an algorithm for efficient prediction of Casimir interactions among arbitrary materials in arbitrary geometries. *Phys Rev A* 88:022514. <https://doi.org/10.1103/PhysRevA.88.022514>
- Rodriguez AW, Capasso F, Johnson SG (2011) The Casimir effect in microstructured geometries. *Nat Photonics* 5:211–221. <https://doi.org/10.1038/nphoton.2011.39>
- Roux P, Woïrgard E, Pizzi M, De MO, Koniachkine V (2005) Fem modelling of an electro-optical micro-shutter. *Sensors Actuators A Phys* 119:1–7. <https://doi.org/10.1016/j.sna.2004.06.022>
- Schalberger P, Al Nusayer SA, Raichle C (2016) 54–I: Parallel fabrication for integration of electronic and microelectromechanical systems. *SID Symp Dig Tech Pap* 47:731–734. <https://doi.org/10.1002/sdtp.10737>
- Schlam E, Finch J, Koskulics J (2017) Highly reflective electrostatic shutter display. In: proceedings of the conference international display workshops. Sendai, Japan
- Takahashi M, Figus C, Malfatti L, Tokuda Y, Yamamoto K, Yoko T, Kitanaga T, Tokudome Y, Innocenzi P (2012) Strain-driven self-rolling of hybrid organic–inorganic microrolls: interfaces with self-assembled particles. *NPG Asia Mater* 4:e22–e22. <https://doi.org/10.1038/am.2012.40>
- Tang L, Wang M, Ng CY, Nikolic M, Chan CT, Rodriguez AW, Chan HB (2017) Measurement of non-monotonic Casimir forces between silicon nanostructures. *Nat Photonics* 11:97–101. <https://doi.org/10.1038/nphoton.2016.254>
- Tarraf A, Daleiden J, Irmer S, Prasai D, Hillmer H (2004) Stress investigation of PECVD dielectric layers for advanced optical MEMS. *J Micromech Microeng* 14:317–323. <https://doi.org/10.1088/0960-1317/14/3/001>
- Tian Z, Veerasubramanian V, Bianucci P, Mukherjee S, Mi Z, Kirk AG, Plant DV (2011) Single rolled-up InGaAs/GaAs quantum dot microtubes integrated with silicon-on-insulator waveguides. *Opt Express* 19:12164. <https://doi.org/10.1364/oe.19.012164>
- Tolias P (2020) Non-retarded room temperature Hamaker constants between elemental metals. *Surf Sci* 700:121652. <https://doi.org/10.1016/j.susc.2020.121652>
- Ueltzhöffer T, Streubel R, Koch I, Holzinger D, Makarov D, Schmidt OG, Ehresmann A (2016) Magnetically patterned rolled-up exchange bias tubes: a paternoster for superparamagnetic beads. *ACS Nano* 10:8491–8498. <https://doi.org/10.1021/acs.nano.6b03566>
- Wang M, Tang L, Ng CY, Messina R, Guizal B, Crosse JA, Antezza M, Chan CT, Chan HB (2021) Strong geometry dependence of the Casimir force between interpenetrated rectangular gratings. *Nat Commun* 12:600. <https://doi.org/10.1038/s41467-021-20891-4>
- Xi W, Schmidt CK, Sanchez S, Gracias DH, Carazo-Salas RE, Jackson SP, Schmidt OG (2014) Rolled-up functionalized nanomembranes as three-dimensional cavities for single cell studies. *Nano Lett* 14:4197–4204. <https://doi.org/10.1021/nl4042565>
- Xu L, Shyu TC, Kotov NA (2017) Origami and Kirigami nanocomposites. *ACS Nano* 11:7587–7599. <https://doi.org/10.1021/acs.nano.7b03287>
- Zhao R, Li L, Yang S, Bao W, Xia Y, Ashby P, Wang Y, Zhang X (2019) Stable Casimir equilibria and quantum trapping. *Science* 364:984–987. <https://doi.org/10.1126/science.aax0916>
- Zhu G, Levine J, Praly L, Peter Y-A (2006) Flatness-based control of electrostatically actuated MEMS with application to adaptive optics: a simulation Study. *J Microelectromech Syst* 15:1165–1174. <https://doi.org/10.1109/JMEMS.2006.880198>

**Publisher's Note** Springer Nature remains neutral with regard to jurisdictional claims in published maps and institutional affiliations.